scientific reports

Check for updates

OPEN

A field-deployable diagnostic assay for the visual detection of misfolded prions

Peter R. Christenson[1,2], Manci Li[2,3], Gage Rowden[2,3], Marc D. Schwabenlander[2,3], Tiffany M. Wolf[2,4], Sang-Hyun Oh[1,2]✉ & Peter A. Larsen[2,3]✉

Diagnostic tools for the detection of protein-misfolding diseases (i.e., proteopathies) are limited. Gold nanoparticles (AuNPs) facilitate sensitive diagnostic techniques via visual color change for the identification of a variety of targets. In parallel, recently developed quaking-induced conversion (QuIC) assays leverage protein-amplification and fluorescent signaling for the accurate detection of misfolded proteins. Here, we combine AuNP and QuIC technologies for the visual detection of amplified misfolded prion proteins from tissues of wild white-tailed deer infected with chronic wasting disease (CWD), a prion disease of cervids. Our newly developed assay, MN-QuIC, enables both naked-eye and light-absorbance measurements for detection of misfolded prions. MN-QuIC leverages basic laboratory equipment that is cost-effective and portable, thus facilitating real-time prion diagnostics across a variety of settings. In addition to laboratory-based tests, we deployed to a rural field-station in southeastern Minnesota and tested for CWD on site. We successfully demonstrated that MN-QuIC is functional in a non-traditional laboratory setting by performing a blinded analysis in the field and correctly identifying all CWD positive and CWD not-detected deer at the field site in 24 h, thus documenting the portability of the assay. White-tailed deer tissues used to validate MN-QuIC included medial retropharyngeal lymph nodes, parotid lymph nodes, and palatine tonsils. Importantly, all of the white-tailed deer (n = 63) were independently tested using ELISA, IHC, and/or RT-QuIC technologies and results secured with MN-QuIC were 95.7% and 100% consistent with these tests for positive and non-detected animals, respectively. We hypothesize that electrostatic forces help govern the AuNP/prion interactions and conclude that MN-QuIC has great potential for sensitive, field-deployable diagnostics for CWD, with future potential diagnostic applications for a variety of proteopathies.

A common feature of many neurodegenerative diseases is the presence of misfolded proteins that accumulate within the central nervous system, ultimately contributing to advanced neurodegeneration and death. Misfolded protein diseases (proteopathies) impact a wide variety of mammals, including Creutzfeldt-Jakob disease (CJD), Alzheimer's disease, and Parkinson's disease in humans, bovine spongiform encephalopathy (BSE) in cattle, scrapie in sheep, pituitary pars intermedia dysfunction (PPID) in horses and chronic wasting disease (CWD) in cervids[1–5]. Given well-documented diagnostic limitations surrounding proteopathies in both animals and humans, (i.e., poor sensitivity, limited antibodies for immuno-based assays, etc.), it is imperative to develop improved diagnostic assays[2,6–11]. With respect to prion diseases (a proteopathy subclass caused by infectious proteins), tests that could be deployed in a variety of settings (e.g., hospitals, veterinary clinics, food processing plants, field stations, etc.) would greatly aid the detection of infectious prions thus limiting their spread. It is within this framework that we approach the development of diagnostic tools for CWD of cervids, a model neurodegenerative disorder with urgent needs for portable diagnostic assays that would facilitate rapid detection, thus preventing CWD prions from entering human and animal food-chains.

Similar to CJD in humans, which progresses rapidly and is always fatal, and BSE in cattle, CWD is a prion disease or Transmissible Spongiform Encephalopathy (TSE) that is 100% fatal to infected animals and has no treatments or prevention methods[1,12]. CWD impacts cervids across North America, Scandinavia, and South

[1]Department of Electrical and Computer Engineering, University of Minnesota, Minneapolis, MN 55455, USA. [2]Minnesota Center for Prion Research and Outreach (MNPRO), University of Minnesota, St. Paul, MN 55108, USA. [3]Department of Veterinary and Biomedical Sciences, University of Minnesota, St. Paul, MN 55108, USA. [4]Department of Veterinary Population Medicine, University of Minnesota, St. Paul, MN 55108, USA. ✉email: sang@umn.edu; plarsen@umn.edu

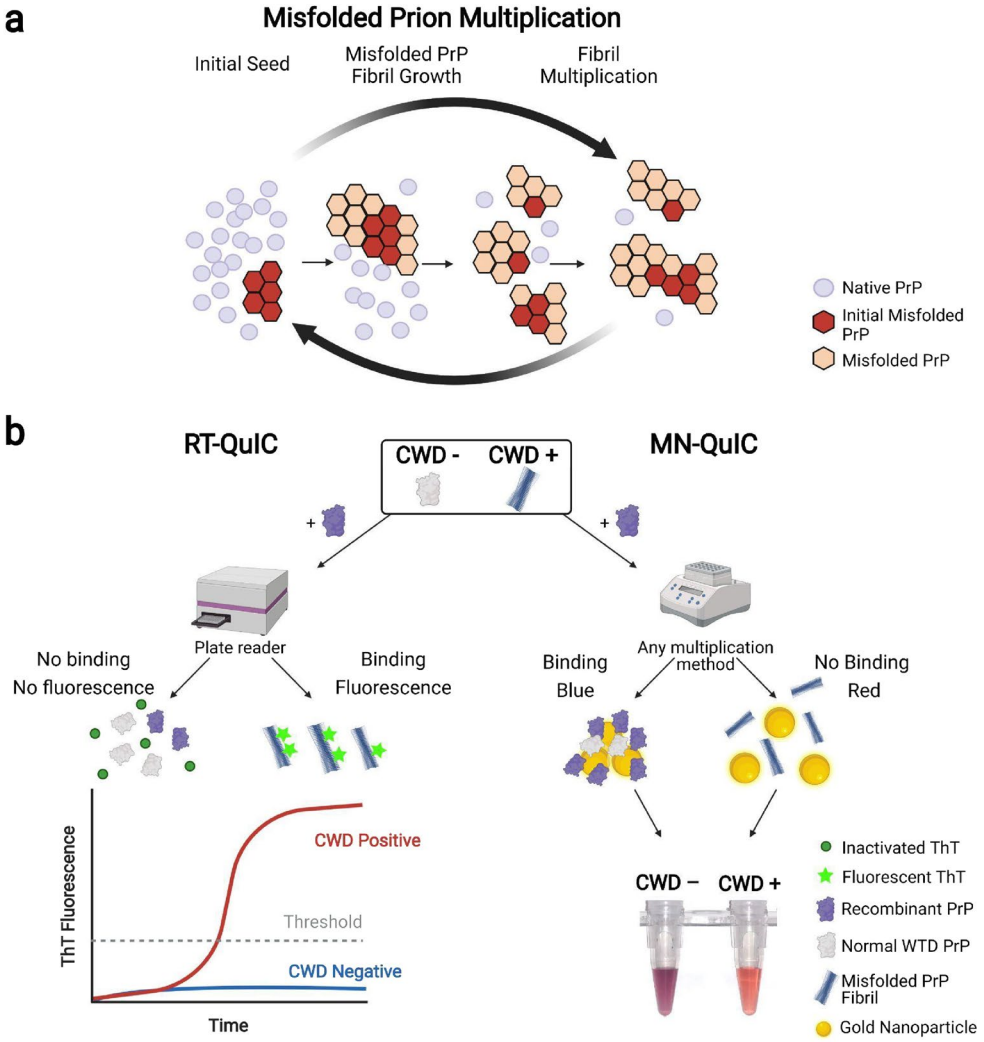

Figure 1. Overview of prion fibril multiplication and two prion amplification assays. (**a**) Schematic of misfolded prion fibril growth. The initial misfolded PrP (PrP^{CWD}) causes native PrP to misfold. (**b**) Overview of RT-QuIC and MN-QuIC. RT-QuIC: Seeds originating from tissue samples of cervids (whether CWD negative or CWD positive) are added to recombinant PrP solutions. These solutions are then shaken and incubated for ~ 48 h (depending on sample type). If present, misfolded PrP fibrils (PrP^{CWD}) from CWD positive tissue induce conformational changes of the recombinant PrP. Amplification results are read in real-time with ThT fluorescence. MN-QuIC: After 24 h amplification, products are diluted and added to an AuNP solution. CWD positive samples result in a red solution (peak absorbance wavelength ~ 516 nm) while CWD negative solutions are blue/purple (peak absorbance wavelength ~ 560 nm).

Korea[13,14] (e.g., elk, moose, mule deer, white-tailed deer, reindeer). The disease continues to spread to new cervid populations, and there are increasing health concerns for both humans and animals exposed to various CWD prion strains[13–15]. All mammals have native functioning cellular prion protein (PrP) distributed throughout various tissues and playing essential roles in a variety of physiological functions, especially those of the central nervous system[16]. Like other protein misfolding neurodegenerative disorders, native prions in cervids adopt conformations of misfolded prions (PrP^{CWD}) (Fig. 1a). PrP^{CWD} propagates throughout an infected animal, forming fibrils that accumulate in lymph and nervous tissues, leading to death years after exposure. CWD poses risks to the health of impacted cervid populations globally, and the disease is an immediate threat to not only cervid health, but also all cervid-related economies. Indeed, cervid hunting and related activities generate tens of billions of USD annually in the United States alone[17]. Across the world, cervids provide a wide array of economically/medicinally[18] important products that are routinely consumed and/or used by humans (i.e., venison meat, antler velvet health supplements, antlers, hides, etc.).

Current diagnostic methods for the detection of protein-misfolding diseases, including CWD and other TSEs, are limited[2,6–11]. Commonly utilized TSE diagnostic assays rely heavily on antibody-based enzyme-linked immunosorbent assay (ELISA) and immunohistochemistry (IHC) technologies that are expensive, time-consuming, and require substantial training and expertise to operate[6]. In addition, a major limitation of ELISA and IHC

Method	Amplification	Time of Amplification	Measurement	Signal Type	Detector	References
MN-QuIC	Thermomixer	24 h	End point	Color change (AuNP)	Naked eye	This work
EP-QuIC	Thermomixer	24–48 h	End point	Fluorescence (ThT)	Fluorometer	[22,23]
RT-QuIC	Plate reader	24–48 h	Continuous real time monitoring	Fluorescence (ThT)	Fluorometer	[6,24–27]

Table 1. Comparison among quaking amplification assays.

assays is that the antibodies routinely used cannot differentiate between native PrP and misfolded TSE-associated prion proteins (PrP^{TSE}) thus requiring protein digestion to enrich for PrP^{TSE}, a methodology that may impact diagnostic sensitivity through the destruction of particular TSE-affiliated PrP strains[19,20]. Collectively, these antibody-based assays are limited in the identification of early-stage TSE infections, and they are primarily used on tissues collected post-mortem.

The detection of prion seeding activity was recently enhanced by various assays involving the amplification of protein misfolding in vitro, including protein misfolding cyclic amplification (PMCA)[6,21], end-point quaking-induced conversion (EP-QuIC)[22,23] and real-time quaking-induced conversion (RT-QuIC)[6,24–27]. Of these prion amplification methods, both EP-QuIC and RT-QuIC (Fig. 1b) utilize a recombinant mammalian PrP substrate (rPrP) that is incubated and shaken with the diagnostic samples. When PrP^{TSE} is present within a given QuIC reaction, it induces a conformational change of the rPrP, forming a beta-sheet enriched mixture that is quantified with fluorescent Thioflavin T (ThT) measurements. Despite the advantages of EP-QuIC and RT-QuIC, there still remain major limitations, including the need for expensive and large laboratory equipment and complex strategies for visualizing and analyzing results, thus limiting access to diagnostic tests. In short, more effective TSE diagnostic methods that leverage small and portable equipment with easily interpretable results are needed to rapidly detect various TSEs in widespread surveillance and prevent additional spread and introduction of TSE prions into human and animal food chains. This is especially true for CWD, as the disease continues to expand across both farmed and wild cervid populations.

In parallel to diagnostic advancements based on prion and protein amplification methods, gold nanoparticles (AuNPs) have been increasingly used for medical applications including disease diagnostics[28–30], drinking water safety[31], and food safety[32]. Due to localized surface plasmon resonances (density fluctuation of conduction electrons)[33], AuNPs have optical absorption peaks that are sensitive to the environment at the AuNP's surface[33–37]. These unique optical properties make plasmonic nanoparticles useful in color-based detection assays[38,39]. Previous studies have indicated affinities of prion proteins with a variety of bare and functionalized metals, including gold[39–42]. One limitation of AuNPs is that they are susceptible to nonspecific binding[43]. Real biological samples are not homogeneous and have many different proteins, ions, and other organic molecules associated with them that can induce AuNPs to spontaneously aggregate making effective AuNP diagnostics challenging. To overcome this, we sought to demonstrate the diagnostic utility of gold nanoparticles for detecting misfolded PrP^{CWD} within QuIC amplified products of CWD positive and negative white-tailed deer (WTD) tissues in homogeneous recombinant hamster prion protein substrates.

By combining the unique plasmonic properties of AuNPs and the methods of quaking-based prion protein fibril amplification, we have successfully overcome the challenges associated with AuNP diagnostics in biological samples and have produced a nanoparticle-based assay (herein named Minnesota-QuIC; MN-QuIC) that can detect the presence or absence of misfolded PrP^{CWD} using both visual and spectroscopic methods (Fig. 1b; Table 1). This method uses only basic lab equipment which reduces assay cost and facilitates deployment outside a traditional laboratory setting. In March of 2021, we deployed the MN-QuIC assay to a field station in rural southeastern Minnesota where the Minnesota Department of Natural Resources (DNR) was performing its annual CWD surveillance and targeted culling efforts. We demonstrated proof-of-concept experiments for MN-QuIC's utility as a portable prion assay by successfully detecting CWD-infected WTD tissues at the DNR field station.

Results

Gold nanoparticle interaction with native cellular prions vs. misfolded fibrils. To investigate whether AuNPs can differentiate between misfolded PrP fibrils and native PrP originating from recombinant hamster prion protein (rPrP), two sets of reaction mixtures seeded with and without spontaneously misfolded rPrP prion fibrils were processed following modified RT-QuIC protocols without ThT[44,45]. The presence of fibril formation was examined in all reaction mixtures by adding and quantifying ThT post hoc (Fig. S1a). ThT fluorescence was significantly different between misfolded rPrP (seeded) and native non-misfolded rPrP (no seed) ($p = 0.05$; Fig. S1a). We hypothesized that misfolded prion fibrils would interact differently with AuNPs, as compared with native rPrP, and that the interaction would influence AuNP aggregation as measured by dynamic light scattering (DLS). Following ThT quantification, misfolded rPrP samples and native rPrP samples were spiked into separate AuNP solutions. After a 30 min incubation period at ambient temperature, there was a visible color difference between the AuNP solutions spiked with misfolded and native rPrP similar to the change in Fig. 1b. This was also reflected in the visible spectrum of the absorbance peak (Fig. 2a).

Color changes due to AuNP aggregation have been reported in the literature for a variety of nanoparticle/protein combinations[38,39]. DLS experiments were performed on three AuNP solutions (seeded, non-seeded, and blank; see Methods), and average effective particle size was determined for each sample (Fig. 2b). We observed a significant difference of AuNP effective particle sizes between AuNP solutions seeded with misfolded rPrP

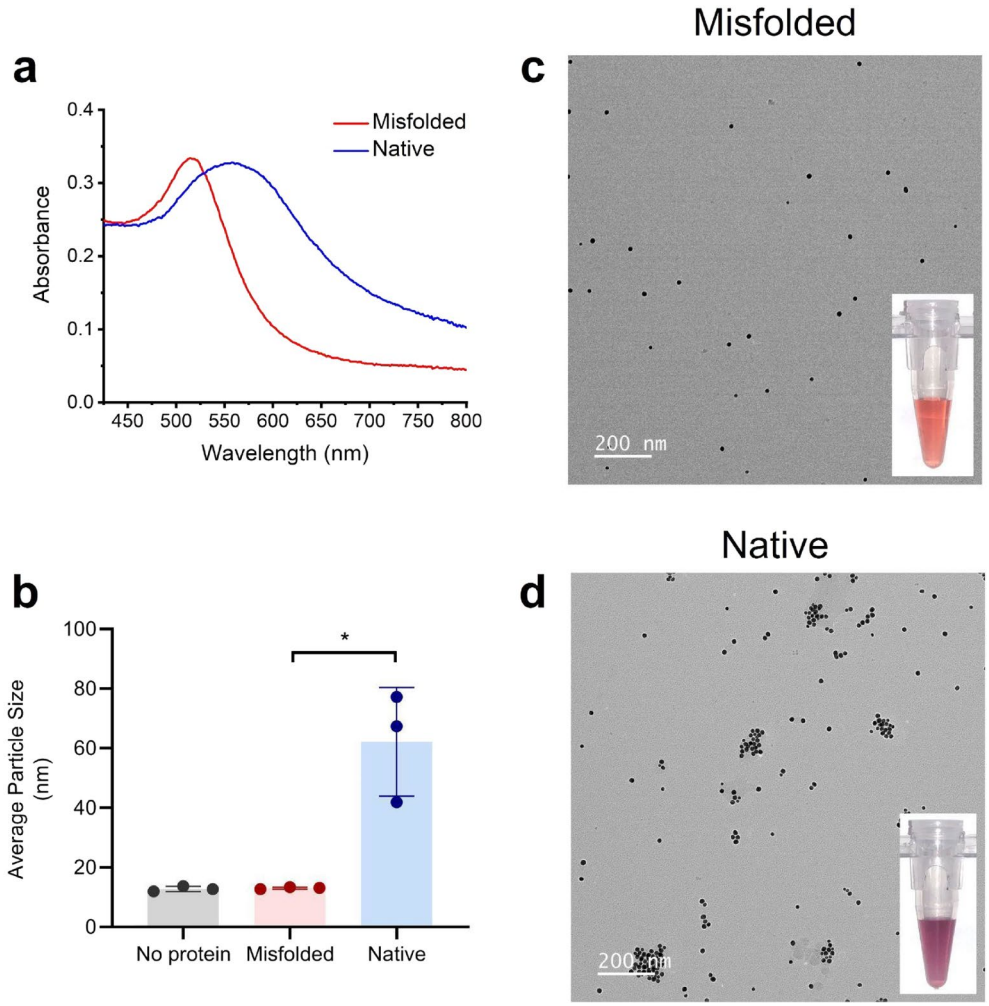

Figure 2. Mechanism of AuNP solution color shift. (**a**) The absorbance spectrum of AuNP solutions spiked with misfolded rPrP from seeded QuIC reactions (red line) and native (non-misfolded) rPrP from QuIC reactions without seed (blue line). (**b**) Average effective particle sizes in AuNP solutions containing no protein, misfolded rPrP, and native rPrP observed by DLS. (**c**) TEM image of 15 nm AuNPs after being spiked with post amplified misfolded PrP. Inset shows an example of AuNP solution after being spiked with misfolded PrP. (**d**) TEM image of aggregating AuNPs after being spiked with native PrP. Inset shows an example of AuNP solution after being spiked with post amplified native PrP. *, p-value < 0.05, error bars show standard deviation.

versus native non-seeded rPrP ($p = 0.05$) (Fig. 2b). The AuNPs spiked with no protein (blank) and misfolded rPrP exhibited similar particle size distributions (Fig. S1b,c), indicating that the misfolded rPrP solutions did not induce AuNP aggregation. On the contrary, the addition of diluted native rPrP resulted in larger particle sizes for AuNPs (Fig. S1d) than AuNPs with no protein added (Fig. S1b), indicating that the addition of diluted native rPrP caused AuNPs to aggregate. To further examine this, AuNP solutions spiked with spontaneously misfolded rPrP and native rPrP were studied in a transmission electron microscope (TEM). Through TEM, it was clear that the AuNPs did not aggregate when spiked with misfolded prion (Fig. 2c). Conversely, it could be seen that AuNPs aggregate in the presence of native rPrP (Fig. 2d). These results were consistent with DLS measurements and indicate differential AuNP binding interaction between native rPrP and misfolded rPrP fibrils.

CWD positive and negative samples produce unique AuNP optical signatures. Understanding that misfolded prions can induce rPrP misfolding and subsequent amplification[46], thus influencing AuNP aggregation (see above), we then investigated the potential of MN-QuIC for CWD diagnostics using PrP^{CWD} positive and negative WTD lymphoid tissues. We used homogenates of independently confirmed CWD positive and negative WTD medial retropharyngeal lymph nodes (RPLN) (Table S1). Independent RT-QuIC analyses were performed on all tissues used for AuNP analyses (Fig. 3a)[27].

In light of our previous results, we anticipated that AuNPs could be utilized to facilitate direct visualization of QuIC-amplified misfolded rPrP solutions that were seeded with CWD positive tissue using a standard benchtop thermomixer. Because thermomixers are more cost effective and have a smaller footprint than plate readers, they have been used previously in conjunction with end-point ThT readings (i.e., EP-QuIC) to determine the

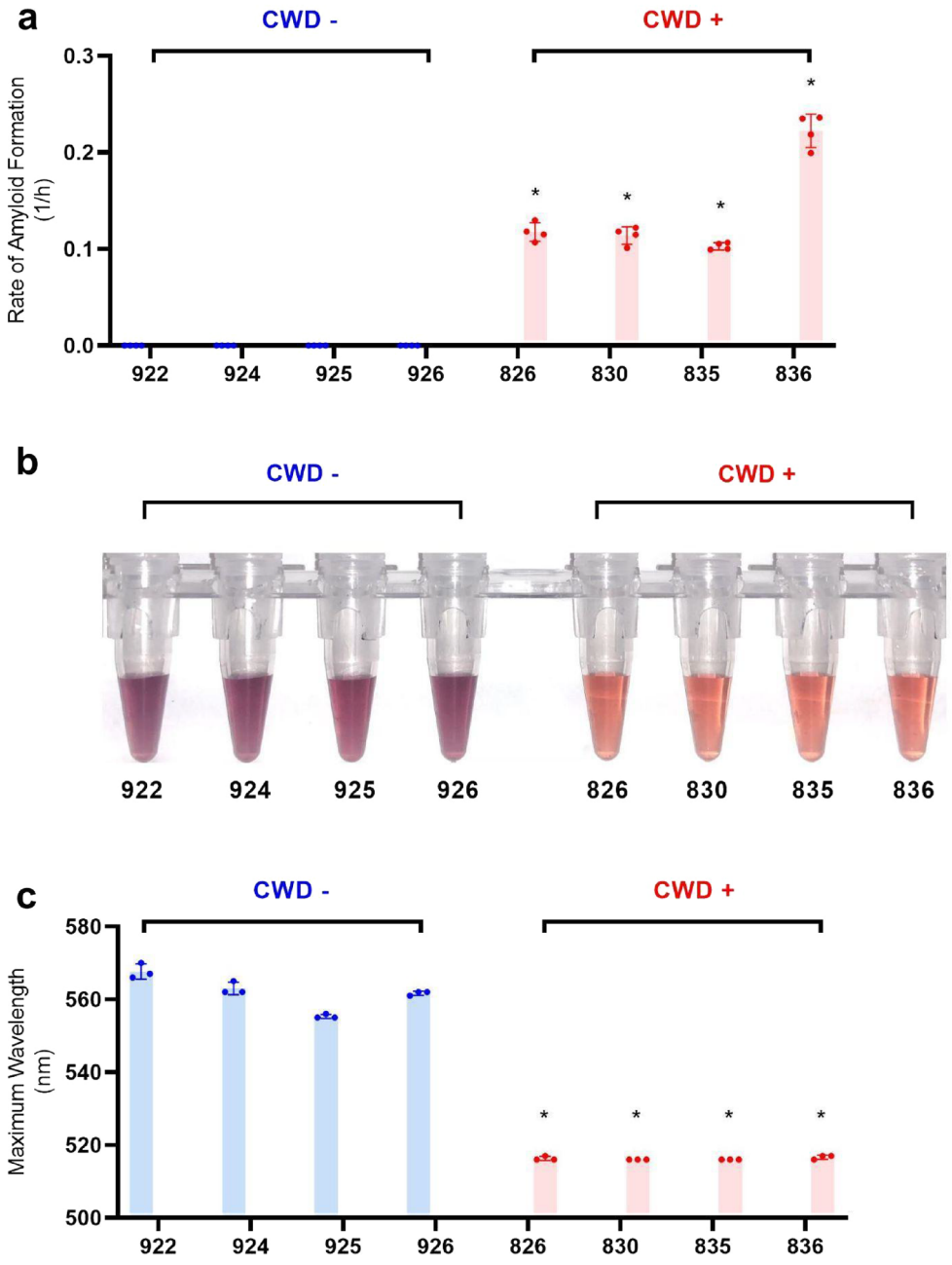

Figure 3. Comparison of RT-QuIC and MN-QuIC results for CWD positive and negative RPLN tissues. MNPRO sample identification number on the horizontal axis. (**a**) RT-QuIC data for the rate of amyloid formation for negative and positive RPLN tissue samples from wild WTD using ThT fluorescence. (**b**) Photo of MN-QuIC tubes showing the color difference for the same set of tissue samples used in (**a**). (**c**) MN-QuIC peak absorbance wavelength of the same set of solutions used in (**b**). *p-value < 0.05, error bars show standard deviation.

presence of CJD prion seeding activity[22,23]. To test this, homogenates from the same set of samples tested with RT-QuIC (Fig. 3a.) were added to the RT-QuIC master mix without ThT on 96-well plates, which were then subjected to shaking/incubation cycles on a thermomixer for 24 h. The post-amplification solutions were then diluted to 50% in buffer and added to AuNP solutions. We found that we were able to clearly distinguish CWD positive and negative samples simply through color difference appreciable by naked eye; the QuIC-amplified CWD positive and negative samples were red and purple, respectively (Fig. 3b).

To quantify our observations and measure statistical differences, the absorbance spectrum of the AuNPs was measured from 400 to 800 nm using a 96-well plate reader. In the resulting absorbance spectrum, AuNP solutions combined with QuIC-amplified CWD positive samples had absorbance peaks near 516 nm (Fig. 3c), similar to the 515 nm absorbance peak of the AuNPs prior to the addition of protein solutions. However, the negative

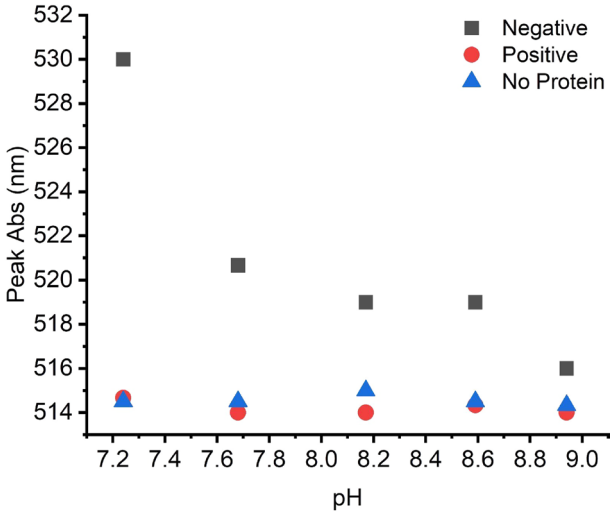

Figure 4. Wavelength of peak absorbance of AuNPs in varying pH buffers containing CWD negative rPrP (square), CWD positive (PrP^{CWD}) (circle), and blank/no protein (triangle) solutions.

sample absorbance peaks were shifted to longer wavelengths of approximately 560 nm (Fig. 3c), confirming that the purple color of AuNP solutions from QuIC products originating from CWD negative tissue samples was consistent with the observed purple color of AuNP aggregates associated with native rPrP (Fig. 2b and Fig S1d). Accordingly, the peak AuNP absorbance wavelengths of CWD negative samples are significantly larger ($p < 0.05$) than CWD-positive samples (Fig. 3c).

Electrostatic forces and rPrP concentration play a role in AuNP-based CWD detection. Considering the results described above, we aimed to determine the mechanism underlying AuNP aggregation caused by native rPrP solutions. Studies of prions and other proteins have shown that electrostatic forces help govern the interactions between nanoparticles and proteins[39,47,48]. Because the theoretical isoelectric point (pI) of our rPrP is around pH 8.9[49], rPrP is positively charged in the pH 7.4 AuNP buffer whereas citrate capped AuNPs are negatively charged even at pHs well below our buffer[50]. Thus at pH 7.4, there exists an electrostatic attractive force between AuNPs and native rPrP that contributes to their interactions (AuNP aggregation and the color change). The charge on the protein changes when the pH of the environment is altered and thus the interaction between AuNP and rPrP is disrupted. When the pH of a solution is raised closer to the IP of the rPrP, the charge of the protein will become closer to neutral, decreasing the force of attraction between AuNP and rPrP. We showed that as the pH of the AuNP solution was raised closer to the IP of native rPrP, the absorbance peak of the AuNP-rPrP solution decreased from 530 nm (Fig. 4) while the control AuNP solution with no protein had very little peak deviation from 515 nm. This indicates that electrostatic interactions were partially responsible for facilitating the native rPrP interactions with AuNPs. QuIC-amplified PrP^{CWD} products, on the other hand, have experienced major conformational changes from their native form (as confirmed by ThT beta-sheet binding; Fig. 3a) and have formed fibrils. These fibrils can further clump to form large tangled structures, reducing the effective concentration of rPrP in the reaction. When there is a low concentration of free-floating rPrP in the solution, the interaction between prions and AuNPs drops below detectable levels (Fig. S2). Because of the concentration effects from large fibril formation, the interaction between positive (misfolded) prions and AuNPs is unaltered by pH (Fig. 4).

Field deployment and high-throughput protocols. To show the potential for a portable, field-deployable diagnostic, we performed proof-of-concept experiments at a rural Minnesota DNR field station (Fig. 5a). We tested both pooled and individual tissues consisting of medial retropharyngeal lymph nodes, parotid lymph nodes, and palatine tonsils tissues from 13 WTD that the DNR had recently collected from the surrounding wild deer population. Three of these animals (blinded to the field team) were CWD positive as determined by regulatory ELISA and IHC testing of medial retropharyngeal lymph nodes. Using a blinded testing approach, MN-QuIC successfully detected all three CWD positive animals via visibly red AuNP solutions (Fig. 5b). We obtained CWD not detected or negative results (purple AuNP solutions) for the 10 animals that were independently identified by ELISA as CWD not detected (Table S2). These proof-of-concept experiments demonstrate the potential utility of MN-QuIC as a portable, field-deployable diagnostic tool for researchers and agencies.

Through field deployment, we conceived and developed a high-throughput protocol for MN-QuIC. In order to examine its reliability, a blinded set of an additional 20 CWD negative and 20 CWD positive WTD RPLNs (Table S3) were tested in a 96-well format in the laboratory. The CWD status of these tissues was independently confirmed by ELISA and/or IHC. For MN-QuIC, each sample had eight replicates and was prepared and subjected to the QuIC protocol using a 96-well plate on a thermomixer for 24 h. A multichannel pipette was then used to add the QuIC amplified protein to a separate 96-well plate filled with AuNP solution and subsequent

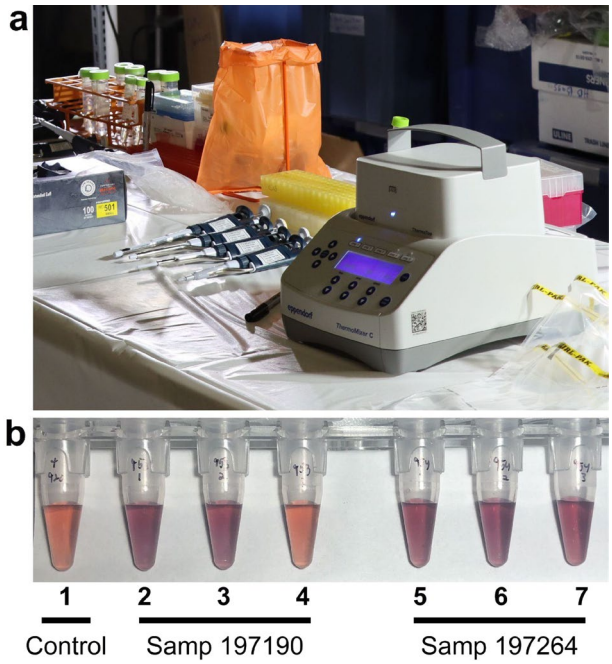

Figure 5. Images from experiments performed in the field. (**a**) Portable MN-QuIC setup used during field deployment. (**b**) Example of observed visible color of the MN-QuIC reaction when testing for CWD. Far-left tube (Tube 1) is a positive control, followed by CWD not-detected tube (in purple; Tubes 2, 3, 5, 6, 7) and a single CWD positive tube (in red; Tube 4). Tubes 2–4 correspond to animal 197190 in Table S2 and tubes 5–7 correspond to animal 197264 in Table S2.

color changes were observed within the first minute. For RT-QuIC analyses, it is common practice to consider a particular sample positive if 50% or more of its wells are positive[24,51–53]. Using this approach, we successfully identified 18 out of 20 CWD positive tissues and 20 out of 20 CWD negative tissues in the blinded sample set using MN-QuIC (Table S3).

To show MN-QuIC's versatility with other tissue types, palatine tonsils from a set of 10 CWD negative and 10 CWD positive WTD (Table S4) were tested using the same protocol used for the blinded set of 40 RPLNs (eight AuNP replicates in a 96-well plate). The CWD status of the palatine tonsil tissues was independently confirmed with RT-QuIC (Fig. 6a). CWD positive samples were identified using a threshold of 50% or more of wells being red (i.e., majority red in color), and we correctly identified 100% of CWD positive samples with no false positives using the MN-QuIC assay (Fig. 6b; Tables S4, S5). In addition to visual color, these results were assessed by investigating the peak shift from the expected 517 nm (red) for positive samples and all red wells had absorbance peaks within 4 nm of 517 nm.

Sensitivity, specificity and serial dilutions. Table S5 reports the sensitivity and specificity for each individual sample set tested herein. Overall sensitivity and specificity of MN-QuIC compared to RPLN ELISA/IHC, when combining all animals from the sample sets presented in Tables S1-S4, was found to be 95.7% (95% confidence interval = 79–99%) and 100% (95% confidence interval = 91–100%), respectively. To examine the lower limit of CWD detection for MN-QuIC, two 96-well plates with serial dilutions (8 replicates each) of a CWD positive parotid lymph node ranging from 10^{-1} to 10^{-8} were created and shaken/incubated for 24 h on a thermomixer (MN-QuIC) and plate reader (RT-QuIC), respectively. Within 24 h both MN-QuIC and RT-QuIC detected seeding for replicate(s) from 10^{-2} to 10^{-6} (Table 2). Interestingly, RT-QuIC was unable to detect PrP^{CWD} seeding activity at a 10^{-1} dilution (eight replicates with no amyloid formation), perhaps due to a higher concentration of inhibitors (vs. 10^{-2}, etc.). However, four of eight replicates for the 10^{-1} dilution were positive using MN-QuIC.

Discussion

Given the continued spread of CWD among cervid populations throughout North America, Northern Europe, and South Korea[13,14] there is an urgent need to develop widely accessible diagnostic tools for CWD. Historically, AuNP colorimetric assays have been limited because of spontaneous AuNP aggregation issues when used with biological samples[43]. Here, we combined QuIC amplification of CWD prions with the simplicity of gold nanoparticles to effectively eliminate spontaneous AuNP aggregation challenges and to enable the visualization of positive vs. negative CWD lymph node and palatine tonsil WTD samples. We hypothesized that the conformational differences between the native rPrP substrate and misfolded prion fibrils would influence the aggregation of AuNPs in solution.

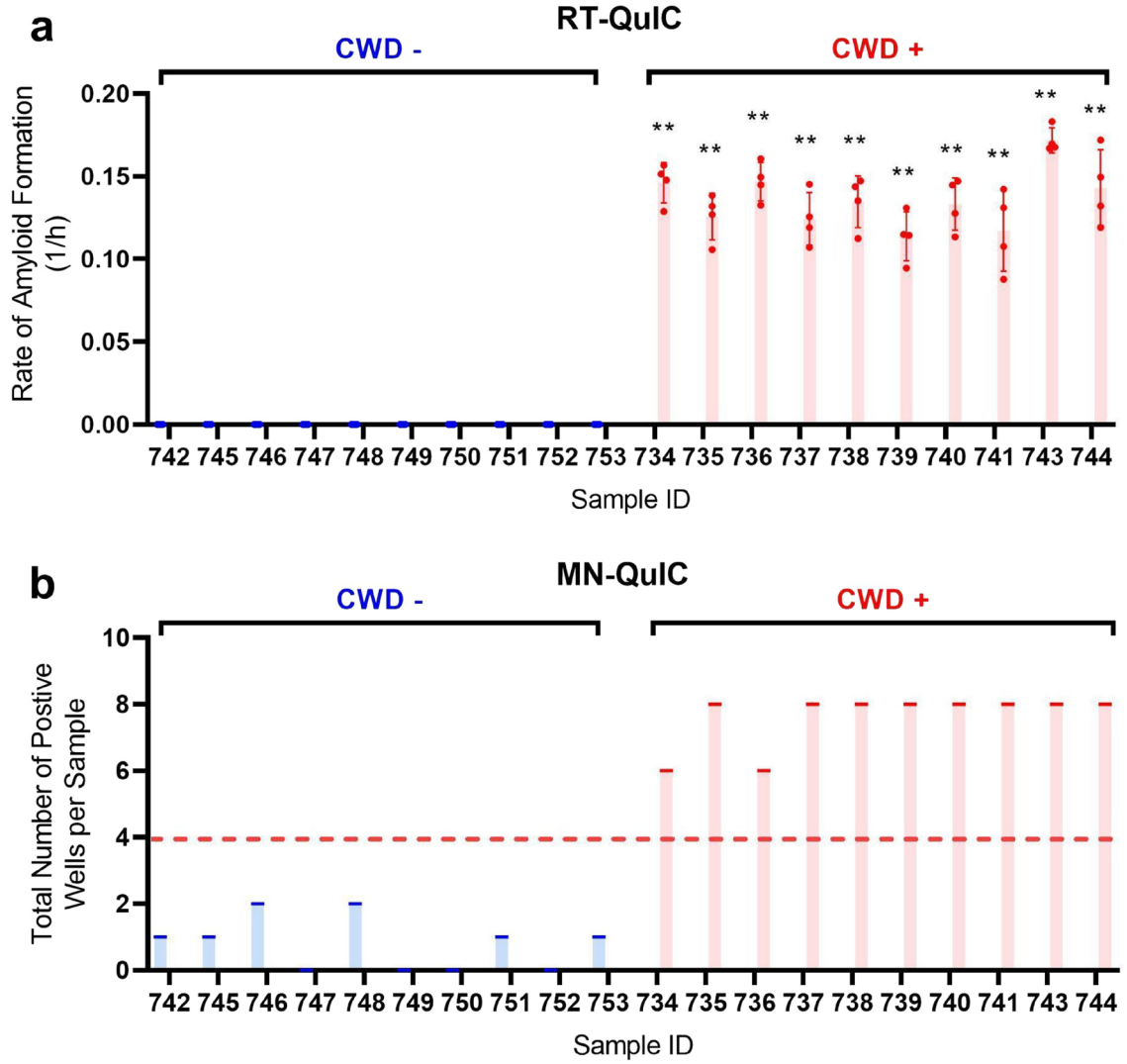

Figure 6. Comparison of RT-QuIC and MN-QuIC results for CWD positive and negative palatine tonsil tissues. MNPRO sample process identification number on horizontal axes (**a**). Fluorescent RT-QuIC data for tissues (see Supplementary Table S4) used in (**b**). (**b**) MN-QuIC data for tonsil samples used in this study. Number of red wells out of the 8 replicates for each sample tested. Following published RT-QuIC protocols (see Results and discussion) 50% or more of MN-QuIC red wells are identified as CWD positive and less than 50% of MN-QuIC red wells as CWD not detected or negative. $^{**}p < 0.01$, error bars show standard deviation.

Dilution Factor	Number of Replicates with Seeding Detected via MN-QuIC	Number of Replicates with Seeding Detected via RT-QuIC
10^{-1}	4	0
10^{-2}	8	8
10^{-3}	8	8
10^{-4}	8	8
10^{-5}	4	8
10^{-6}	1	8
10^{-7}	0	0
10^{-8}	0	0

Table 2. Serial dilution: Dilutions of CWD positive parotid lymph node run for 24 h via MN-QuIC vs 24 h via RT-QuIC.

By injecting post-QuIC-amplified protein solutions into AuNPs, we were able to clearly distinguish (via visible color change) between CWD positive and CWD negative medial retropharyngeal lymph node and palatine tonsil tissues. AuNP solutions for these positive and negative samples appeared red and purple, respectively. We further confirmed that the color change was a result of the aggregation of AuNPs by conducting DLS and TEM experiments that compared the effective particle sizes in the presence of native and misfolded rPrP. We observed that the AuNP aggregation was governed by electrostatic interactions by altering the pH of the solution. Finally, we demonstrated proof-of-concept experiments for the practical utility of MN-QuIC by successfully identifying CWD-infected WTD tissues at a DNR field station in southeastern MN.

We estimated the sensitivity and specificity of MN-QuIC for CWD detection (across several tissue types from individual WTD) in comparison to diagnosis by ELISA/IHC using RPLNs, the standard of practice for CWD diagnosis in WTD (Table S5)[27]. It is important to note that where tissue types differ, we are not only comparing diagnostic test performance, but also the probability that a certain tissue type will contain detectable levels of PrP^{CWD} as compared to RPLN. Yet, tissue distribution of PrP^{CWD} can vary based on route of infection, stage of infection, and prion strain[54–56]. We also recognize that under conditions of natural infection, the assumption that ELISA and IHC are a "gold standard" for diagnostic test comparison may be inappropriate given that these tests are imperfect[57]. Knowing these limitations, estimates of diagnostic test performance warrant further evaluation using methods that can overcome the constraints related to reliance on a "gold standard" comparison[57–60].

Dilution experiments comparing MN-QuIC and RT-QuIC after 24 h reveal that both MN-QuIC and RT-QuIC can detect signs of PrP^{CWD} seeding activity down to 10^{-6} homogenate solutions (Table 2). It should be noted that RT-QuIC had more replicates detect seeding at low dilutions than MN-QuIC. However, this could be due to the exclusion of N-2 supplement from MN-QuIC homogenate dilutions in this study due to concerns that it may affect prion–AuNP interaction. N-2 coats the walls of RT-QuIC dilution tubes which aids the detection of extremely low prion content. The observation that both methods detected PrP^{CWD} seeding down to 10^{-6} dilutions is significant because it suggests that MN-QuIC has similar sensitivity to RT-QuIC.

Of all samples tested, there were only two CWD positive RPLNs (sample process IDs 923 and 926) where MN-QuIC was not consistent with ELISA or RT-QuIC results (Table S3). For these samples, two of eight replicates turned red and thus using the 50% red well threshold were classified as PrP^{CWD} not-detected via MN-QuIC in contrast to a CWD positive classification from ELISA and RT-QuIC testing. However it should be noted that when independently tested, the RPLN from sample 923 exhibited low ELISA optical density (OD) and a low rate of amyloid formation on RT-QuIC, likely indicating relatively low levels of PrP^{CWD} within the tissue. Using MN-QuIC, sample 926 (animal ID 832) was found to be negative on RPLN (Table S3), however MN-QuIC identified this same animal (animal ID 832) as positive on palatine tonsils (Table S4). Tissue sampling variability, particularly with low levels of PrP^{CWD}, can affect test outcome when using uni-lateral sampling (i.e., testing only the left RPLN) or different subsamples from the same tissue[61].

The primary laboratory equipment for MN-QuIC consists of a tissue homogenizer, temperature-controlled shaker, and if desired (but not necessary), a spectrometer for light absorbance readings in addition to visual observations. Compared to EP-QuIC/RT-QuIC and PMCA, which leverage ThT fluorescence and antibody-based Western blotting, respectively[6], results from MN-QuIC can be visualized with the naked eye or quantified using simply light-absorbance readings. Because MN-QuIC is a protein amplification method, it can be adapted to examine any tissue or biological sample that existing and future RT-QuIC protocols use, thus giving MN-QuIC wide versatility. Studies have shown that amplification-based assays, such as RT-QuIC, are more sensitive than conventional ELISA[62]. Given that MN-QuIC has similar sensitivity to RT-QuIC (Table 2) and uses a similar amplification method, MN-QuIC has the potential to have increased sensitivity compared to ELISA. Recent publications have used specially functionalized AuNPs to detect a variety of protein targets[39,63–65]. However, the AuNPs used here are capped with citrate, which is one of the most common methods for stabilization making it simple and widely commercially available. For this reason, MN-QuIC offers a cost-effective approach to CWD testing as less than $1.00 USD of AuNPs are used per sample (including 8 replicates). When including reagent and production costs for recombinant hamster protein, the approximate MN-QuIC cost per sample is nearly the same as RT-QuIC (~ $12.00 to $15.00 USD per sample; four to eight replicates). At the time of publication, the cost of equipment for MN-QuIC is just 20% (~ $6000 USD) of that which is needed for RT-QuIC (~ $30,000 USD) and slightly over 50% of that used in low-throughput ELISA (~ $11,000 USD). By eliminating the need for time consuming preparation and/or the relatively expensive visualization strategies used in EP-QuIC, RT-QuIC, ELISA, IHC and/or PMCA, MN-QuIC provides new opportunities for widely accessible and sensitive CWD diagnostics.

AuNPs have been used in a variety of advanced sensing applications[28,29,31–33,66,67]. Our work demonstrates that AuNPs can open promising avenues for the identification of misfolded prions. Because prion proteins have strong interactions with simply functionalized metallic surfaces, besides AuNPs, we envision a broad range of metallic nanoparticles with various materials and shapes to be useful in detection. Additionally, substrate-based nanostructures exhibiting optical resonances could be useful in detecting conformational changes via other sensing modalities such as surface-enhanced infrared absorption spectroscopy[68,69] to further improve the speed and accuracy of prion detection. Examining other areas of the electromagnetic spectrum, such as tera-Hertz sensing, could also lead to improved detection[70].

To demonstrate field deployment capabilities of the MN-QuIC assay, we collected medial retropharyngeal lymph nodes, parotid lymph nodes, and palatine tonsil samples from 13 WTD at a rural DNR field station. Using both pooled and individual tissues of these 13 individuals, MN-QuIC was 100% successful in identifying three CWD positive and 10 CWD not-detected animals. The successful field-based classification of these animals provides clear proof-of-concept demonstration of MN-QuIC's utility as a portable and sensitive field test. We note that our MN-QuIC analysis has a low false-negative rate, and has yet to produce a statistically significant false positive result. These observations are critically important when considering MN-QuIC as a field-based

diagnostic tool for CWD. Moreover, any positive result can be independently validated using downstream RT-QuIC, ELISA, and/or IHC testing. Given growing concerns of CWD prion strain variation and risks to human and animal health[15], any field-based diagnostic assay that avoids producing false-negative is preferred.

RPLN and palatine tonsils collected from WTD were the basis for the laboratory-based analyses conducted herein because these tissues are ideal for early and accurate identification of CWD infection, with tonsils additionally having antemortem applications[27,71]. Future studies should be performed using MN-QuIC on large sample sets to better characterize MN-QuIC's sensitivity and specificity for specific tissues. Additional work will focus on leveraging MN-QuIC for CWD diagnostics using a variety of antemortem biological samples (e.g., blood, saliva, and feces). RT-QuIC amplification assays using samples acquired from living deer have recently been reported[45,72] and these assays could be readily combined with MN-QuIC to provide field-deployable antemortem tests of both wild and farmed cervids. Moreover, MN-QuIC may have potential food-safety test applications given the recent documentation of RT-QuIC-based detection of CWD prions in WTD muscles used for human and animal consumption[26].

The mechanisms underlying interactions between AuNPs and various prion proteins are underexplored, given the results reported herein a detailed characterization of AuNP–prion interactions is highly desirable. Based on the available knowledge in the field, we hypothesized that as the pH approaches the prion's isoelectric point, the electrostatic force of attraction between the negatively charged citrate capped AuNP and the protein would decrease. Our analyses revealed that as the pH neared the theoretical isoelectric point of rPrP, the wavelength of the peak absorbance of the AuNPs spiked with native (CWD negative) protein decreased. We also found that pH alterations had little effect on AuNP solutions without protein, indicating that the effect of pH on native rPrP-spiked AuNP solutions was not caused by intrinsic AuNP aggregation in response to the changing pH. QuIC-amplified CWD positive solutions did not change with varying pH because of fibril formation effects on free-floating prion concentration. Therefore, the difference in interactions between CWD negative and positive solutions is likely governed by electrostatic forces and rPrP concentration effects. However, other factors such as hydrophobic interactions[73,74] could also play a role. Various studies have shown that both native and misfolded PrP bind various metal ions and bulk metals including gold[16,40–42]. Our research reveals AuNPs stabilized with a simple citrate capping readily interact with the truncated rPrP substrate that is used as the primary substrate for a growing variety of QuIC assays. Future structural analyses focused on native rPrP and prion fibrils[75] could provide further insight into how native rPrP, but not misfolded rPrP fibrils, influence AuNP aggregation.

Conclusions

MN-QuIC holds great promise not only for the visual detection of CWD-positive samples but also for the detection of other protein misfolding diseases. The need for inexpensive, sensitive, widely deployable diagnostics for neurodegenerative diseases is only growing as neurodegenerative diseases are predicted to greatly increase in the next decades[2,76]. It has been proposed that advances in CWD diagnostics will yield technologies that are useful for a broad range of neurodegenerative diseases[6]. RT-QuIC protocols have already been developed for a number of sample types allowing for antemortem tests[45,72]. These and future amplification methods could readily be combined with MN-QuIC. Additionally, QuIC amplification protocols have been developed for a variety of other protein misfolding diseases including scrapie in sheep[77], BSE in cattle[78], and Alzheimer's[79], Parkinson's[52,80], and CJD in humans[22,23]. Thus, we posit that the combination of AuNP technology with protein amplification assays has great potential for the development of versatile neurodegenerative disease diagnostic platforms. By eliminating the need for expensive/complicated visualization schemes, our hybrid assay technology has the potential to greatly increase access to neurodegenerative disease diagnostics. It is our vision that in the future, variations of this AuNP-based protein amplification/detection assay could be deployed in medical clinics around the world to aid in neurodegenerative diagnosis and early application of therapeutics.

Methods

Tissue preparation. 60 WTD tissues (30 CWD-negative and 30 CWD-positive; from 50 animals) were selected for laboratory-based RT-QuIC and MN-QuIC analyses (Tables S1, S3, S4 and S5). These samples were collected from WTD through collaboration with the Minnesota DNR (Schwabenlander et al.[27]; Tables S1, S3 and S4), and their CWD status was independently identified utilizing the Bio-Rad TeSeE Short Assay Protocol (SAP) Combo Kit (BioRad Laboratories Inc., Hercules, CA, USA). Positive RPLNs were confirmed by IHC at the Colorado State University Veterinary Diagnostic Laboratory. Metadata containing information of all specimens examined in the lab, including tissue type, is provided in supplementary materials (Tables S1, S3 and S4). Supporting Table S5 provides a summary of the MN-QuIC results used in this study and their classification compared to independent testing. WTD RPLNs (Tables S1 and S3) and palatine tonsils (Table S4) were homogenized in PBS (10% w:v) in 2 mL tubes containing 1.5 mm zirconium beads with a BeadBug Homogenizer (Benchmark Scientific, Sayreville New Jersey, USA) on max speed for 90 s. These samples are referred to as 10% homogenates. All CWD positive and negative samples were selected based on independent ELISA, IHC, and/or RT-QuIC results and were subsampled using methods as reported in Schwabenlander et al.[27].

Preparation of recombinant substrate. Recombinant hamster PrP (HaPrP90-231) production and purification followed the methods in Schwabenlander et al.[27] The substrate is derived from a truncated form (amino acids 90–231) of the Syrian hamster PRNP gene cloned into the pET41-a(+) expression vector and was expressed in Rosetta (DE3) *E. coli*. The original clone was provided by the National Institutes of Health Rocky Mountain Laboratory. Many studies have utilized haPrP for RT-QuIC[7,26,27,44,45]. Recombinant hamster PrP was used in this study due to its seemingly universal proclivity to misfold in the presence of infectious prions for a large variety of species.

QuIC for lymph tissues. For QuIC analysis (both MN-QuIC and RT-QuIC), a master mix was made to the following specifications: 1X PBS, 1 mM Ethylenediaminetetraacetic acid (EDTA), 170 mM NaCl, 10 µM thioflavin T (ThT), and 0.1 mg/mL rPrP. In instances where the end reaction would be analyzed using AuNPs, ThT could be excluded. The 10% tissue homogenates (prepared as described above) were further diluted 100-fold in 0.1% Sodium Dodecyl Sulfate (SDS) using methods from Schwabenlander et al.[27] (final tissue dilution: 0.1%). 1ul of N-2 Supplement [Life Technologies Corporation, Carlsbad, California, USA]) was added to 99ul dilution of SDS (for MN-QuIC reactions N-2 was excluded from SDS). 2 µL of the diluent were added to each well containing 98 uL of master mix. Plates for RT-QuIC were amplified on a FLUOstar® Omega plate reader (BMG Labtech, Cary, North Carolina, USA; 42 °C, 700 rpm, double orbital, shake for 57 s, rest for 83 s). Fluorescent readings were taken at ~ 45 min increments.

Thermomixer-based amplification. For MN-QuIC, we leveraged a standard benchtop shaking incubator (thermomixer) to produce QuIC-based prion amplifications as previously reported by Cheng et al.[22] and Vendramelli et al.[23], although with slight modifications. Plates were prepared identically to those amplified on the plate reader (see protocol above). Instead of shaking on a plate reader, reactions were performed on a ThermoMixer® C equipped with SmartBlock plate and Thermotop (Eppendorf, Enfield, Connecticut, USA) at 48 °C for 24 h at 600 RPM (60 s shake and 60 s rest). We selected a 24 h run time based on independent RT-QuIC results for RPLNs and palatine tonsils from CWD positive WTD reported in Schwabenlander et al.[27], including those examined herein, showing significant seeding activity within 9 to 24 h (Fig. S3). The resultant products were visualized with the addition of gold nanoparticles (as described below).

Spontaneous misfolding of rPrP for DLS Experiment. Spontaneous misfolding of recombinant prion protein was generated similarly standard RT-QuIC but with unfiltered recombinant proteins and reagents. For these reactions, no infectious seed was necessary. The spontaneously misfolded material was used to seed reactions for the dynamic light scattering experiment, described below.

Preparation of gold nanoparticles. Post-amplified material was visualized with 15 nm citrate-capped gold nanoparticles purchased from Nanopartz (Loveland, Colorado, USA) with stock concentrations ranging from 2.45 nM to 2.7 nM. AuNP protocols were modified from Špringer et al.[81] and Zhang et al.[39] AuNPs were buffer exchanged using 530ul of stock solution that was centrifuged in 1.6 mL tubes at 13,800 g for 10 min. 490ul of supernatant was removed and the undisturbed pellet was resuspended with 320ul of a low concentration phosphate buffer (PBS_{low}; pH 7.4 via addition of HCl) made of 10 mM Na_2HPO_4(Anhydrous), 2.7 mM KCl, 1.8 mM KH_2PO_4). After the quaking/incubation steps, protein solutions were diluted to 50% in MN-QuIC buffer (pH 7.2), consisting of 1X PBS with the addition of final concentrations of 1 mM EDTA, 170 mM NaCl, 1.266 mM sodium phosphate. Forty microliters of the protein diluted 50% in MN-QuIC buffer were then added to the 360ul AuNP solution with ample mixing (results shown in Fig. 3b,c). This solution was left to react at room temperature (RT) for 30 min (although a visible color change is observable within 60 s) before visual color was recorded (purple or red) and photographed. After images were taken, three replicates of 100ul were taken from the 400ul AuNP mixture and pipetted into three separate wells of a 96-well plate. The absorbance spectrum was then recorded for each well at wavelengths 400–800 nm using the FLUOstar® Omega plate reader (BMG Labtech, Cary, North Carolina, USA).

For AuNP visualization experiments performed to determine higher throughput capacity (Fig. 6; Tables S3, S4), proteins were prepared in the same way. After amplification on the thermomixer, proteins on a 96-well plate were diluted to 50% using MN-QuIC buffer and a multichannel pipette. 90ul of AuNPs were then added to a separate non-binding 96-well plate. The AuNP wells were spiked with 10ul of the diluted protein from the thermomixer (post-amplification) using a multichannel pipette. After waiting 30 min, the color changes were observed and the absorbance spectrum of the plate was taken.

Dynamic light scattering. Spontaneously misfolded rPrP samples (described above) were produced from solutions of rPrP with no seed added. In addition to these samples, a 96-well RT-QuIC reaction was performed with half the wells consisting of native rPrP seeded with spontaneously misfolded rPrP, and half consisting of native rPrP with no seed. The 96-well plate was then amplified using QuIC protocols described above. Post-amplification, seeded samples were confirmed to have fibrillation while the non-seeded samples were confirmed to not have fibrillation based on ThT binding (described above). Seeded and non-seeded samples were diluted to 50% in MN-QuIC buffer, and 40ul of these solutions were added to 360ul of AuNPs in PBS_{low}. Additionally, a blank with no protein was produced by adding 40ul of MN-QuIC buffer to 360ul of AuNPs in PBS_{low}. For native rPrP samples, color change was observed within 1 min of rPrP addition. No color change was observed in spontaneously misfolded rPrP samples at any time length. Dynamic light scattering measurements of all samples were taken after 5 min of protein addition using a Microtract NanoFlex Dynamic Light Scattering Particle Analyzer (Verder Scientific, Montgomeryville, PA, USA), and measurement times were 60 s. Five measurements were taken for each sample and then averaged.

TEM measurements. TEM measurements were performed using a Tecnai G2 F30 Transmission Electron Microscope. Images were recorded on a Gatan K2 Summit direct electron detector. 20ul of post-amplified positive and negative rPrP were added to separate volumes of 200ul of AuNPs prepared as described above. Each protein solution was added to separate uncharged TEM grids. Stain was not used because it was unnecessary to view the AuNPs.

Effects of pH and rPrP substrate concentration on the AuNP-protein interaction. In order to test the effects of pH on the interaction of rPrP with AuNP, five different 10 mM tris-buffer solutions with pHs ranging from 7.2 to 9.0 were created. Tris was used to give buffering for the desired pH range. AuNPs were buffer exchanged as described above except tris-buffer was used instead of PBS_{low}. Protein solutions were added as previously described. It can be noted that the peak absorbance for the tris buffer solution below pH 7.4 is still not as high as the peak shifts in pH 7.4 PBS_{low}. This is likely due to the differences in tris and PBS_{low} buffers.

To examine effects of rPrP substrate concentration (Fig. S2), six different master mixes were made with concentrations of native rPrP ranging from 0 mg/ml to 0.1 mg/ml. 10ul of each solution were added to separate wells containing 90ul AuNPs (pH 7.4 AuNPs prepared as described above).

Additional statistical information. We estimated Wilson Score confidence intervals for MN-QuIC sensitivity and specificity estimates in Epitools[82]. Wilson confidence intervals are appropriate for small sample sizes when values of p are close to 0 or 1[83]. Note for sensitivity calculations, Animal 832 was considered positive because of it's MN-QuIC tonsil result (Table S4). GraphPad Prism version 9.0 for Windows (GraphPad Software, San Diego, California USA, www.graphpad.com) was used for conducting statistical analysis. Three technical replicates were used to demonstrate the potential application of AuNP on spontaneously misfolded rPrP. For initial trials on RPLN tissues from eight (four positive and four negative) animals, four and three technical replicates were used for RT-QuIC and AuNPs, respectively. For plate-based protocols, we tested palatine tonsils from ten positive and ten negative animals using four and eight replicates for RT-QuIC and AuNPs, respectively. We also tested 40 medial retropharyngeal lymph nodes (20 CWD positive and 20 CWD negative; Table S3) using four and eight replicates for RT-QuIC and AuNPs, respectively. Unless specified in figures, rate of amyloid formation and maximum wavelength of samples were compared to negative controls on their respective plate. The one-tailed Mann–Whitney unpaired u-test ($\alpha = 0.05$) was used to test the average difference for all parameters of interests between samples.

Field deployment. In March of 2021, we collaborated with the Minnesota DNR during annual CWD surveillance of the wild WTD population in Fillmore and Winona Counties, Minnesota. We assembled the necessary MN-QuIC equipment as described above on two portable tables within a DNR facility in Rushford, MN. RPLNs, parotid lymph nodes, and palatine tonsils were collected as described in Schwabenlander et al.[27], and were sampled and pooled together for each of the 13 animals tested. Tissues were homogenized in a BeadBug™ 3 Microtube homogenizer. All tissues were subject to 24 h MN-QuIC protocols as described above. Three replicates were performed for each of the 13 tissue pools and, for field-based analyses, a tissue pool was considered suspect CWD positive if one or more replicates was red. Tissues for suspected positive tissue pools were tested individually (Table S2). A tissue pool was considered CWD not-detected if all three replicates were blue or purple.

Animal research statement. No white-tailed deer were euthanized specifically for the research conducted herein and all tissues were secured from dead animals or loaned for our analyses. For these reasons, the research activities conducted herein are exempt from review by the University of Minnesota Institutional Animal Care and Use Committee (as specified https://research.umn.edu/units/iacuc/submit-maintain-protocols/overview). White-tailed deer were euthanized for annual culling efforts to control the spread of CWD in Minnesota following Minnesota Department of Natural Resources state regulations and euthanasia guidelines established by the Animal Care and Use Committee of the American Society of Mammalogists[84]. All methods and all experimental procedures carried out during the course of this research followed University of Minnesota guidelines and regulations as approved by the Institutional Biosafety Committee under protocol #1912-37662H. This study was also carried out in compliance with the ARRIVE guidelines (https://arriveguidelines.org).

Field research. White-tailed deer were euthanized by the state of Minnesota for routine annual culling efforts to control the spread of CWD and were not sampled specifically for the current study. Tissue samples were provided by the Minnesota Department of Natural Resources.

Data availability

All data generated or analyzed during this study are included in this published article and its supplementary information.

Received: 14 April 2022; Accepted: 8 July 2022
Published online: 18 July 2022

References

1. Prusiner, S. B. Nobel lecture: Prions. *Proc. Natl. Acad. Sci. USA* **95**, 13363–13383 (1998).
2. Telling, G. C. Breakthroughs in antemortem diagnosis of neurodegenerative diseases. *Proc. Natl. Acad. Sci. USA* **116**, 22894–22896 (2019).
3. Collinge, J. Prion diseases of humans and animals: Their causes and molecular basis. *Annu. Rev. Neurosci.* **24**, 519–550 (2001).
4. Williams, E. S. & Young, S. Chronic wasting disease of captive mule deer: A spongiform encephalopathy. *J. Wildl. Dis.* **16**, 89–98 (1980).
5. Fortin, J. S. *et al.* Equine pituitary pars intermedia dysfunction: A spontaneous model of synucleinopathy. *Sci. Rep.* **11**, 16036 (2021).
6. Haley, N. J. & Richt, J. A. Evolution of diagnostic tests for chronic wasting disease, a naturally occurring prion disease of cervids. *Pathogens* **6**, 35 (2017).

7. Haley, N. J. *et al.* Chronic wasting disease management in ranched elk using rectal biopsy testing. *Prion* **12**, 93–108 (2018).
8. Martinez, B. & Peplow, P. V. MicroRNAs in Parkinson's disease and emerging therapeutic targets. *Neural Regener. Res.* **12**, 1945–1959 (2017).
9. Hajipour, M. J. *et al.* Advances in Alzheimer's diagnosis and therapy: The implications of nanotechnology. *Trends Biotechnol.* **35**, 937–953 (2017).
10. Figgie, M. P. Jr. & Appleby, B. S. Clinical use of improved diagnostic testing for detection of prion disease. *Viruses* **13**, 789 (2021).
11. Parnetti, L. *et al.* CSF and blood biomarkers for Parkinson's disease. *Lancet Neurol.* **18**, 573–586 (2019).
12. Prusiner, S. B. *et al.* Scrapie prions aggregate to form amyloid-like birefringent rods. *Cell* **35**, 349–358 (1983).
13. Hannaoui, S., Schatzl, H. M. & Gilch, S. Chronic wasting disease: Emerging prions and their potential risk. *PLoS Pathog.* **13**, e1006619 (2017).
14. Joly, D. O. *et al.* Chronic wasting disease in free-ranging Wisconsin White-tailed Deer. *Emerg. Infect. Dis.* **9**, 599–601 (2003).
15. Osterholm, M. T. *et al.* Chronic wasting disease in cervids: Implications for prion transmission to humans and other animal species. *MBio* **10**, e01091-e1119 (2019).
16. Westergard, L., Christensen, H. M. & Harris, D. A. The cellular prion protein (PrPC): Its physiological function and role in disease. *Biochim. Biophys. Acta* **1772**, 629–644 (2007).
17. U.S. Fish and Wildlife Service & U.S. Census Bureau. *2016 National Survey of Fishing, Hunting and Wildlife-Associated Recreation*. https://www.census.gov/library/publications/2018/demo/fhw-16-nat.html (2018).
18. Wu, F. *et al.* Deer antler base as a traditional Chinese medicine: A review of its traditional uses, chemistry and pharmacology. *J. Ethnopharmacol.* **145**, 403–415 (2013).
19. Safar, J. G. *et al.* Prion clearance in bigenic mice. *J. Gen. Virol.* **86**, 2913–2923 (2005).
20. Haley, N. J. *et al.* Sensitivity of protein misfolding cyclic amplification versus immunohistochemistry in ante-mortem detection of chronic wasting disease. *J. Gen. Virol.* **93**, 1141–1150 (2012).
21. Saborio, G. P., Permanne, B. & Soto, C. Sensitive detection of pathological prion protein by cyclic amplification of protein misfolding. *Nature* **411**, 810–813 (2001).
22. Cheng, K. *et al.* Endpoint quaking-induced conversion: A sensitive, specific, and high-throughput method for antemortem diagnosis of Creutzfeldt-Jacob Disease. *J. Clin. Microbiol.* **54**, 1751–1754 (2016).
23. Vendramelli, R., Sloan, A., Simon, S. L. R., Godal, D. & Cheng, K. ThermoMixer-aided endpoint quaking-induced conversion (EP-QuIC) permits faster sporadic Creutzfeldt-Jakob disease (sCJD) identification than real-time quaking-induced conversion (RT-QuIC). *J. Clin. Microbiol.* **56**, e00423-e518 (2018).
24. Cheng, Y. C. *et al.* Early and non-invasive detection of chronic wasting disease prions in elk feces by real-time quaking induced conversion. *PLoS ONE* **11**, e0166187 (2016).
25. Atarashi, R. *et al.* Ultrasensitive human prion detection in cerebrospinal fluid by real-time quaking-induced conversion. *Nat. Med.* **17**, 175–178 (2011).
26. Li, M. *et al.* RT-QuIC detection of CWD prion seeding activity in white-tailed deer muscle tissues. *Sci. Rep.* **11**, 16759 (2021).
27. Schwabenlander, M. D. *et al.* Comparison of chronic wasting disease detection methods and procedures: Implications for free-ranging white-tailed deer (*Odocoileus virginianus*) surveillance and management. *J. Wildl. Dis.* **58**, 50–62 (2021).
28. Tsai, T.-T. *et al.* Diagnosis of tuberculosis using colorimetric gold nanoparticles on a paper-based analytical device. *ACS Sens.* **2**, 1345–1354 (2017).
29. Pelaz, B. *et al.* Diverse applications of nanomedicine. *ACS Nano* **11**, 2313–2381 (2017).
30. Howes, P. D., Chandrawati, R. & Stevens, M. M. Bionanotechnology. Colloidal nanoparticles as advanced biological sensors. *Science* **346**, 1247390 (2014).
31. Thiramanas, R. & Laocharoensuk, R. Competitive binding of polyethyleneimine-coated gold nanoparticles to enzymes and bacteria: A key mechanism for low-level colorimetric detection of gram-positive and gram-negative bacteria. *Microchim. Acta* **183**, 389–396 (2016).
32. Du, X.-J., Zhou, T.-J., Li, P. & Wang, S. A rapid Salmonella detection method involving thermophilic helicase-dependent amplification and a lateral flow assay. *Mol. Cell. Probes* **34**, 37–44 (2017).
33. Mayer, K. M. & Hafner, J. H. Localized surface plasmon resonance sensors. *Chem. Rev.* **111**, 3828–3857 (2011).
34. Myroshnychenko, V. *et al.* Modelling the optical response of gold nanoparticles. *Chem. Soc. Rev.* **37**, 1792–1805 (2008).
35. Lal, S., Link, S. & Halas, N. J. Nano-optics from sensing to waveguiding. *Nat. Photonics* **1**, 641–648 (2007).
36. Sepúlveda, B., Angelomé, P. C., Lechuga, L. M. & Liz-Marzán, L. M. LSPR-based nanobiosensors. *Nano Today* **4**, 244–251 (2009).
37. Dahlin, A. *et al.* Localized surface plasmon resonance sensing of lipid-membrane-mediated biorecognition events. *J. Am. Chem. Soc.* **127**, 5043–5048 (2005).
38. Zhao, W., Brook, M. A. & Li, Y. Design of gold nanoparticle-based colorimetric biosensing assays. *ChemBioChem* **9**, 2363–2371 (2008).
39. Zhang, H.-J. *et al.* Gold nanoparticles as a label-free probe for the detection of amyloidogenic protein. *Talanta* **89**, 401–406 (2012).
40. Flechsig, E. *et al.* Transmission of scrapie by steel-surface-bound prions. *Mol. Med.* **7**, 679–684 (2001).
41. Weissmann, C., Enari, M., Klöhn, P. C., Rossi, D. & Flechsig, E. Transmission of prions. *J. Infect. Dis.* **186**, S157–S165 (2002).
42. Luhr, K. M., Löw, P., Taraboulos, A., Bergman, T. & Kristensson, K. Prion adsorption to stainless steel is promoted by nickel and molybdenum. *J. Gen. Virol.* **90**, 2821–2828 (2009).
43. Masson, J.-F. Surface plasmon resonance clinical biosensors for medical diagnostics. *ACS Sens* **2**, 16–30 (2017).
44. Henderson, D. M. *et al.* Quantitative assessment of prion infectivity in tissues and body fluids by real-time quaking-induced conversion. *J. Gen. Virol.* **96**, 210–219 (2015).
45. Tennant, J. M. *et al.* Shedding and stability of CWD prion seeding activity in cervid feces. *PLoS ONE* **15**, e0227094 (2020).
46. Henderson, D. M. *et al.* Progression of chronic wasting disease in white-tailed deer analyzed by serial biopsy RT-QuIC and immunohistochemistry. *PLoS ONE* **15**, e0228327 (2020).
47. Wang, A., Perera, Y. R., Davidson, M. B. & Fitzkee, N. C. Electrostatic interactions and protein competition reveal a dynamic surface in gold nanoparticle-protein adsorption. *J. Phys. Chem. C* **120**, 24231–24239 (2016).
48. Abel, A. G. B. & Risselada, H. J. Gold-induced fibril growth: The mechanism of surface-facilitated amyloid aggregation. *Angew. Chem. Int. Ed.* **55**, 11242–11246 (2016).
49. Gasteiger, E. *et al.* Protein identification and analysis tools on the ExPASy server. In *The Proteomics Protocols Handbook* 571–607 (Humana Press, 2005).
50. Csapó, E. *et al.* Surface and structural properties of gold nanoparticles and their biofunctionalized derivatives in aqueous electrolytes solution. *J. Dispers. Sci. Technol.* **35**, 815–825 (2014).
51. Haley, N. J., Henderson, D. M., Senior, K., Miller, M. & Donner, R. Evaluation of Winter Ticks (*Dermacentor albipictus*) collected from North American Elk (Cervus canadensis) in an area of chronic wasting disease endemicity for evidence of PrPCWD amplification using real-time quaking-induced conversion assay. *mSphere* **6**, e0051521 (2021).
52. Rossi, M. *et al.* Ultrasensitive RT-QuIC assay with high sensitivity and specificity for Lewy body-associated synucleinopathies. *Acta Neuropathol.* **140**, 49–62 (2020).
53. Mok, T. H. *et al.* Bank vole prion protein extends the use of RT-QuIC assays to detect prions in a range of inherited prion diseases. *Sci. Rep.* **11**, 5231 (2021).

54. Haley, N. J., Mathiason, C. K., Zabel, M. D., Telling, G. C. & Hoover, E. A. Detection of sub-clinical CWD infection in conventional test-negative deer long after oral exposure to urine and feces from CWD+ deer. *PLoS ONE* **4**, e7990 (2009).
55. Spraker, T. R., Balachandran, A., Zhuang, D. & O'Rourke, K. I. Variable patterns of distribution of PrP(CWD) in the obex and cranial lymphoid tissues of Rocky Mountain elk (Cervus elaphus nelsoni) with subclinical chronic wasting disease. *Vet. Rec.* **155**, 295–302 (2004).
56. Sigurdson, C. J., Spraker, T. R., Miller, M. W., Oesch, B. & Hoover, E. A. PrPCWD in the myenteric plexus, vagosympathetic trunk and endocrine glands of deer with chronic wasting disease. *J. Gen. Virol* **82**, 2327–2334 (2001).
57. Picasso-Risso, C. *et al.* Assessment of real-time quaking-induced conversion (RT-QuIC) assay, immunohistochemistry and ELISA for detection of chronic wasting disease under field conditions in white-tailed deer: A Bayesian approach. *Pathogens* **11**, 489 (2022).
58. Chapinal, N., Schumaker, B. A., Joly, D. O., Elkin, B. T. & Stephen, C. Bayesian analysis to evaluate tests for the detection of *Mycobacterium bovis* infection in free-ranging wild bison (Bison bison athabascae) in the absence of a gold standard. *J. Wildl. Dis.* **51**, 619–625 (2015).
59. Branscum, A. J., Gardner, I. A. & Johnson, W. O. Estimation of diagnostic-test sensitivity and specificity through Bayesian modeling. *Prev. Vet. Med.* **68**, 145–163 (2005).
60. Joseph, L., Gyorkos, T. W. & Coupal, L. Bayesian estimation of disease prevalence and the parameters of diagnostic tests in the absence of a gold standard. *Am. J. Epidemiol.* **141**, 263–272 (1995).
61. Bloodgood, J., Kiupel, M., Melotti, J. & Straka, K. Chronic wasting disease diagnostic discrepancies: The importance of testing both medial retropharyngeal lymph nodes. *J. Wildl. Dis.* **57**, 194–198 (2021).
62. McNulty, E. *et al.* Comparison of conventional, amplification and bio-assay detection methods for a chronic wasting disease inoculum pool. *PLoS ONE* **14**, e0216621 (2019).
63. Zhang, X. Gold nanoparticles: Recent advances in the biomedical applications. *Cell Biochem. Biophys.* **72**, 771–775 (2015).
64. Li, J., Yan, X., Li, X., Zhang, X. & Chen, J. A new electrochemical immunosensor for sensitive detection of prion based on Prussian blue analogue. *Talanta* **179**, 726–733 (2018).
65. Zhao, J. *et al.* Graphene oxide-gold nanoparticle-aptamer complexed probe for detecting amyloid beta oligomer by ELISA-based immunoassay. *J. Immunol. Methods* **489**, 112942 (2021).
66. Ruppert, C., Phogat, N., Laufer, S., Kohl, M. & Deigner, H.-P. A smartphone readout system for gold nanoparticle-based lateral flow assays: Application to monitoring of digoxigenin. *Microchim. Acta* **186**, 119 (2019).
67. Mahato, K. *et al.* Gold nanoparticle surface engineering strategies and their applications in biomedicine and diagnostics. *3 Biotech* **9**, 57 (2019).
68. Adato, R. *et al.* Ultra-sensitive vibrational spectroscopy of protein monolayers with plasmonic nanoantenna arrays. *Proc. Natl. Acad. Sci. U. S. A.* **106**, 19227–19232 (2009).
69. Altug, H., Oh, S.-H., Maier, S. A. & Homola, J. Advances and applications of nanophotonic biosensors. *Nat. Nanotechnol.* **17**, 5–16 (2022).
70. Heo, C. *et al.* Identifying fibrillization state of Aβ protein via near-field THz conductance measurement. *ACS Nano* **14**, 6548–6558 (2020).
71. Wild, M. A., Spraker, T. R., Sigurdson, C. J., O'Rourke, K. I. & Miller, M. W. Preclinical diagnosis of chronic wasting disease in captive mule deer (*Odocoileus hemionus*) and white-tailed deer (*Odocoileus virginianus*) using tonsillar biopsy. *J. Gen. Virol.* **83**, 2629–2634 (2002).
72. Ferreira, N. C. *et al.* Detection of chronic wasting disease in mule and white-tailed deer by RT-QuIC analysis of outer ear. *Sci. Rep.* **11**, 7702 (2021).
73. Gao, D. *et al.* Studies on the interaction of colloidal gold and serum albumins by spectral methods. *Spectrochim. Acta A* **62**, 1203–1208 (2005).
74. Szekeres, G. P. & Kneipp, J. Different binding sites of serum albumins in the protein corona of gold nanoparticles. *Analyst* **143**, 6061–6068 (2018).
75. Kraus, A. *et al.* High-resolution structure and strain comparison of infectious mammalian prions. *Mol. Cell* **81**, 4540–4551 (2021).
76. Matthews, K. A. *et al.* Racial and ethnic estimates of Alzheimer's disease and related dementias in the United States (2015–2060) in adults aged ≥65 years. *Alzheimers. Dement.* **15**, 17–24 (2019).
77. Orrú, C. D. *et al.* Human variant Creutzfeldt-Jakob disease and sheep scrapie PrP(res) detection using seeded conversion of recombinant prion protein. *Protein Eng. Des. Sel.* **22**, 515–521 (2009).
78. Hwang, S., Greenlee, J. J. & Nicholson, E. M. Use of bovine recombinant prion protein and real-time quaking-induced conversion to detect cattle transmissible mink encephalopathy prions and discriminate classical and atypical L- and H-Type bovine spongiform encephalopathy. *PLoS ONE* **12**, e0172391 (2017).
79. Kraus, A. *et al.* Seeding selectivity and ultrasensitive detection of tau aggregate conformers of Alzheimer disease. *Acta Neuropathol.* **137**, 585–598 (2019).
80. Fairfoul, G. *et al.* Alpha-synuclein RT-QuIC in the CSF of patients with alpha-synucleinopathies. *Ann. Clin. Transl. Neurol.* **3**, 812–818 (2016).
81. Špringer, T. & Homola, J. Biofunctionalized gold nanoparticles for SPR-biosensor-based detection of CEA in blood plasma. *Anal. Bioanal. Chem.* **404**, 2869–2875 (2012).
82. Sergeant. *Epitools Epidemiological Calculators*. epitools.ausvet.com.http://epitools.ausvet.com.au (2018).
83. Brown, L. D., Tony Cai, T. & DasGupta, A. Interval estimation for a binomial proportion. *Stat. Sci.* **16**, 101–133 (2001).
84. Sikes, R. S. & Animal Care and Use Committee of the American Society of Mammalogists. 2016 Guidelines of the American Society of Mammalogists for the use of wild mammals in research and education. *J. Mammal.* **97**, 663–688 (2016).

Acknowledgements

Funding for research performed herein was provided by the Interdisciplinary Doctoral Fellowship from the University of Minnesota to P.R.C., the Minnesota State Legislature through the Minnesota Legislative-Citizen Commission on Minnesota Resources (LCCMR), Minnesota Agricultural Experiment Station Rapid Agricultural Response Fund, the Sanford P. Bordeau Chair in Electrical Engineering at the University of Minnesota to S.-H.O., and start-up funds awarded to P.A.L. through the Minnesota Agricultural, Research, Education, Extension and Technology Transfer (AGREETT) program. We thank C. Ertsgaard and D. J. Lee for helpful discussions on experimental results and protocols. Portions of this work were conducted in the Minnesota Nano Center, which is supported by the National Science Foundation through the National Nano Coordinated Infrastructure Network (NNCI) under Award Number ECCS-2025124. W. Zhang provided the expertise for TEM studies. Portions of this work were carried out in the University of Minnesota Characterization Facility, which receives partial support from the NSF through the MRSEC (Award Number DMR-2011401) and the NNCI (Award Number ECCS-2025124) programs. F. Schendel, T. Douville, and staff of the University of Minnesota Biotechnology Resource Center provided critical support concerning the large-scale production of recombinant proteins. We thank the Minnesota Department of Natural Resources, especially M. Carstensen, L. Cornicelli, E. Hildebrand, P.

Hagen, and K. LaSharr, for providing the white-tailed deer tissues used for our analyses and logistical assistance for MN-QuIC field deployment. K. Wilson of the Colorado State University Veterinary Diagnostic Laboratory provided assistance with ELISA and IHC testing of samples reported herein. S. Stone provided valuable logistical assistance with our molecular work. We thank NIH Rocky Mountain Labs, especially B. Caughey, A. Hughson, and C. Orru for training and assistance with the implementation of RT-QuIC and for supplying the original rPrP clone. Figure 1 and parts of Fig. 2 were created using BioRender (BioRender.com).

Author contributions

P.R.C. and M.L. conceived the study. P.R.C., M.L., and G.R. performed molecular experiments. P.R.C., M.L., M.S., S.H.O., and P.A.L. assisted with experimental design and interpreted the results. P.R.C., M.L., M.S., T.M.W., and P.A.L. conducted field-based testing of the diagnostics presented herein. P.R.C. and M.L. performed statistical analyses. S.H.O. and P.A.L. oversaw the research. All authors wrote and contributed to the final manuscript.

Competing interests

The authors declare no competing interests.

Additional information

Supplementary Information The online version contains supplementary material available at https://doi.org/10.1038/s41598-022-16323-y.

Correspondence and requests for materials should be addressed to S.-H.O. or P.A.L.

Reprints and permissions information is available at www.nature.com/reprints.

Publisher's note Springer Nature remains neutral with regard to jurisdictional claims in published maps and institutional affiliations.